This project has received funding from the European Union's Horizon 2020 research and innovation programme under under FET-Open grant agreement no. 899646 (k-NET)

DELIVERABLE

Project acronym	k-NET
Project full title	k-Space Neural Computation with magnetic excitations
Grant Agreement no.	899646

Document title	Deliverable 2.1 – Report on the programming by parametric pumping
Revision no.	1
Document date	24/02/2023
Dissemination level	Confidential
Responsible partner	WWU
Contributing partners	WWU, CNRS, CEA
Reviewing partners	All

CHANGE RECORD

Revision	Date	Changes	Authors	Status
1	9/12/2022	version 2	S. O. Demokritov V. E. Demidov G. de Loubens A. Anane J. Ben-Youssef, M. Munoz T. Devolder	Submit-ted

TABLE OF CONTENTS

1 Summary 4
2 Parametric excitation of spin-wave modes 4
2.1 Samples and the experimental technique 4
2.2 Characterization of the parametric excitation process 5
2.3 Dynamic characteristics of the parametric excitation 6
3 Nonlinear interactions of parametrically excited modes 8
3.1 Indirect mode interaction 8
3.2 Nonlinear phase locking of the modes 9
4 PRogramming with parametric pumping stimulation 10
4.1 Observation of spontaneous scattering 10
4.2 Parametric threshold 12
4.3 Scattering stimulated by parametric pumping 13
a) Parametric pumping below or at threshold 13
b) Parametric pumping above threshold 16
5 Conclusion and outlook 17

1 SUMMARY

The ultimate goal of the k-NET is to demonstrate the possibility of utilization of interacting spin-wave eigenmodes for the implementation of neuromorphic computation in the k-space. Within this concept, the discrete spin-wave modes in microscopic magnetic structures play the role of neurons, while the nonlinear interactions among them represent synapses. The implementation of this scheme requires the possibility to excite multiple modes, to drive them into the strongly nonlinear regime, and to independently control their amplitudes. The latter is particularly important, since the inter-mode nonlinear interactions are determined by the amplitudes of the modes. Therefore, programming of synapses in a k-space network requires finding reliable approaches, which allow one to efficiently create a predefined state of the ensemble of interacting modes.

One of the significant difficulties in reaching this controllability is associated with the limitations imposed by the inductive technique traditionally used for the spin-wave excitation. The efficiency of this excitation mechanism depends strongly on the spatial symmetry of the dynamic magnetic field used for the excitation and the spatial distributions of the dynamic magnetization in different spin-wave modes. Since k-NET concentrates on microscopic magnetic structures with lateral dimensions of the order of 1 μm and below, the driving dynamic magnetic field created by the technically feasible excitation elements is nearly uniform across the structure area. Under these conditions, it is impossible to excite modes with anti-symmetric spatial profiles of the dynamic magnetization, while the efficiency of the excitation of symmetric-profile modes quickly decreases with the increase of the mode order.

In order to overcome these limitations, we proposed to utilize the parametric excitation of the modes. In this case, the dynamic magnetic field created by the excitation line is aligned parallel to the static field. As a result, this field does not couple to the spin-wave modes directly. Instead, it can be considered as a dynamic modulation of the static parameter of the system – the strength of the static bias field. Under these conditions, the excitation field is able to induce magnetization dynamics via the parametric-resonance process, when its frequency becomes equal to twice the frequency of a spin-wave mode. Such process is generally known to be free from symmetry limitations and is expected to enable excitation of both symmetric and anti-symmetric modes with the efficiency, which is mostly determined by the relaxation rates of the modes and is nearly independent of the mode spatial distributions. In addition to the efficient excitation, the parametric mechanism is also known to drive the dynamics into the strongly nonlinear regime, which is necessary to achieve nonlinear mode interactions.

Accordingly, within the Task 2.1 of WP2, we planned to study the characteristics of the parametric excitation of the spin-wave modes and their nonlinear interactions in samples designed and fabricated within WP1.

2 PARAMETRIC EXCITATION OF SPIN-WAVE MODES

2.1 Samples and the experimental technique

In the measurements described below, we used the samples prepared within WP1 of the k-NET project, which are described in detail in the technical report D1.1. The spin-wave modes were studied in microscopic disks with the diameter of 1 μm prepared from an Yttrium Iron Garnet (YIG) film with the thickness 66 nm grown by liquid phase epitaxy on a GGG (111) substrate. The parameters of the film were determined within WP1 by using several complementary techniques. These measurements yielded the saturation magnetization $\mu_0 M_s = 176$ mT and the Gilbert damping parameter $\alpha = 8 \times 10^{-5}$. In our studies, the

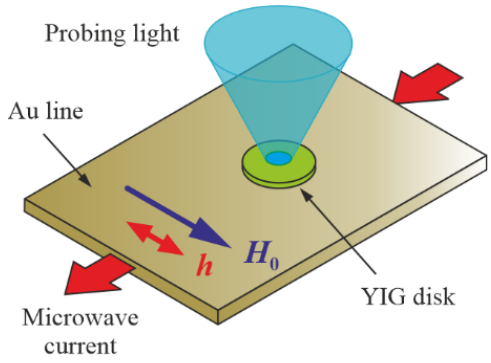

Figure 1: Schematics of the experiment.

excitation of the magnetization dynamics was performed by using lithographically defined Au microwave transmission line with the width of 8 μm and the thickness of 200 nm (Fig. 1). The microwave-frequency current flowing in the line created the dynamic magnetic field *h* oriented perpendicular to the axis of the line. Due to the large ratio between the width of the line and the diameter of the YIG disk, this field was nearly uniform across the disk area. To enable the parametric excitation, the static magnetic field H_0=50 mT was also applied perpendicular to the line axis. Additionally, to compare the parametric and the direct inductive excitation, the field H_0 was slightly rotated to achieve a linear coupling of the dynamic excitation field with the spin-wave modes.

To detect the excited spin-wave modes, we used the micro-focus Brillouin light scattering (BLS) spectroscopy. This technique enables the study of the magnetization dynamics in individual microscopic structures with frequency and temporal resolution. The latter is particularly important for the determination of the characteristic temporal scale of the excitation process and provides reach information about nonlinear mode interactions.

We focused the probing laser light with the wavelength of 473 nm and the power of 0.1 mW into a sub-micrometer diffraction-limited spot on the surface of the YIG disk (Fig. 1) and analysed the modulation of the probing light by magnetization oscillations using a high-contrast optical spectrometer. The obtained signal – the BLS intensity – was proportional to the intensity of magnetic oscillations at a given frequency. By applying the microwave current in a form of short pulses, we additionally got access to the temporal development of the mode intensities after the application of the excitation signal.

2.2 Characterization of the parametric excitation process

Figure 2 shows the comparison of the results achieved by using the direct inductive and the parametric excitation. In the former case, one observes one wide spectral peak centred at the frequency of the fundamental spin-wave mode, while in the latter case, the measured spectrum exhibits a series of well-defined narrow peaks. This result clearly indicates that, in contrast to the inductive excitation, the parametric excitation allows one to efficiently excite many different spin-wave modes and does not suffer from the limitations imposed by the mode symmetries and their spatial distributions. This fact clearly proves the advantages of the parametric excitation mechanism for the implementation of the programing of k-space neural networks.

Figure 3a shows the color-coded map of the intensities of the parametrically excited modes in the frequency-power coordinates, while Fig. 3b presents the sections of this map at several frequencies, as labelled. These data show that the minimum microwave power required for the parametric excitation in the studied system is about 5 mW. At this power, one observes excitation of 3 spin-wave modes. By increasing the power of the parametric pumping signal to 100 mW, one can achieve excitation of up to 15

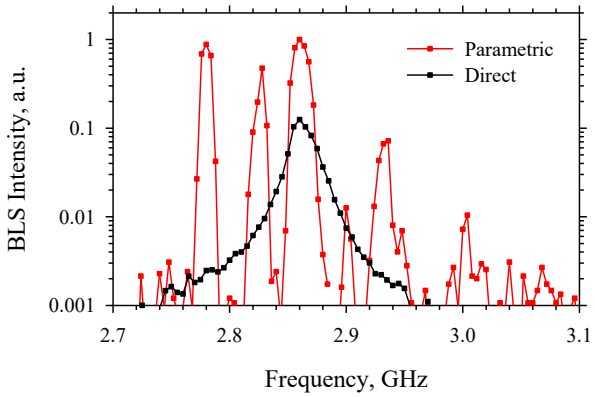

Figure 2: Comparison of the direct inductive and parametric excitation of the spin-wave modes. The data were obtained with the static field rotated by 15 degree.

different modes. The excitation process exhibits a clear threshold behaviour. This threshold is determined by the conditions of the complete compensation of the natural damping of magnetization dynamics by the parametric pumping. The modes at higher frequencies generally require larger power for their excitation due to the increase in the relaxation rate of the magnetization oscillations with increasing frequency. We emphasize that the absolute values of the required microwave power depend on the width of the excitation microwave line. By reducing the latter from 8 μm used in our experiments to 1-2 μm, one can decrease the required power by more than an order of magnitude.

As seen from Fig. 3b, for powers above the threshold, the intensities of the modes quickly saturate. This saturation is caused by the nonlinear effects in the spin system of the magnetic disk and indicates that the modes are driven by the parametric pumping into the strongly nonlinear regime, which is a precondition for the operation of the k-space neural networks.

2.3 Dynamic characteristics of the parametric excitation

Figure 4a shows the temporal dependences of the intensity of the spin-wave mode at the frequency 2.824 GHz for powers of the parametric pumping *P* increasing from 6 to 18 mW in 1 mW step. As seen from these data, after the parametric pumping is applied at *t*=0, the intensity exhibits an exponential increase (note the logarithmic scale of the vertical axis) with the rate, determined by the power *P*. At small powers above the threshold, the growth is relatively slow and the intensity does not show saturation over the

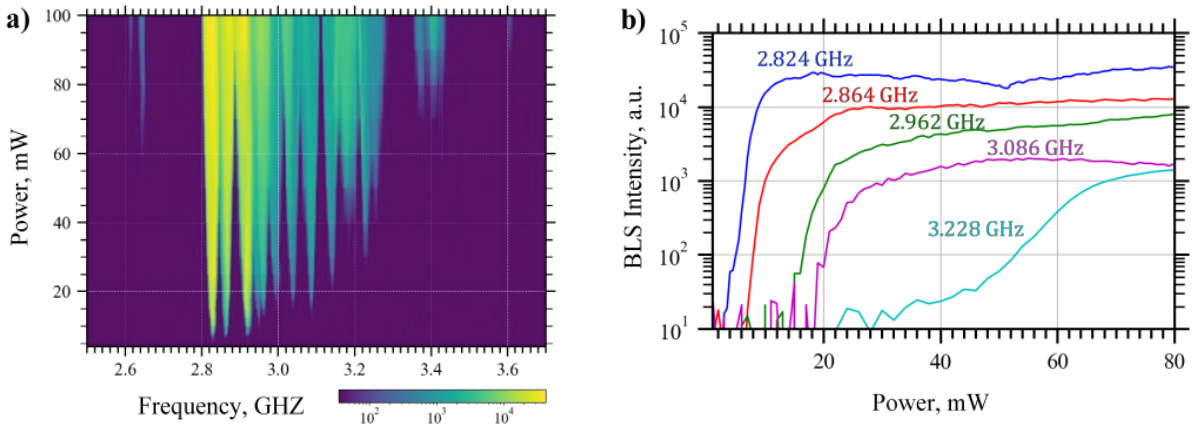

Figure 3: a) Intensity map of the parametrically excited modes in the frequency-power coordinates. b) Sections of the intensity map at the labelled mode frequencies.

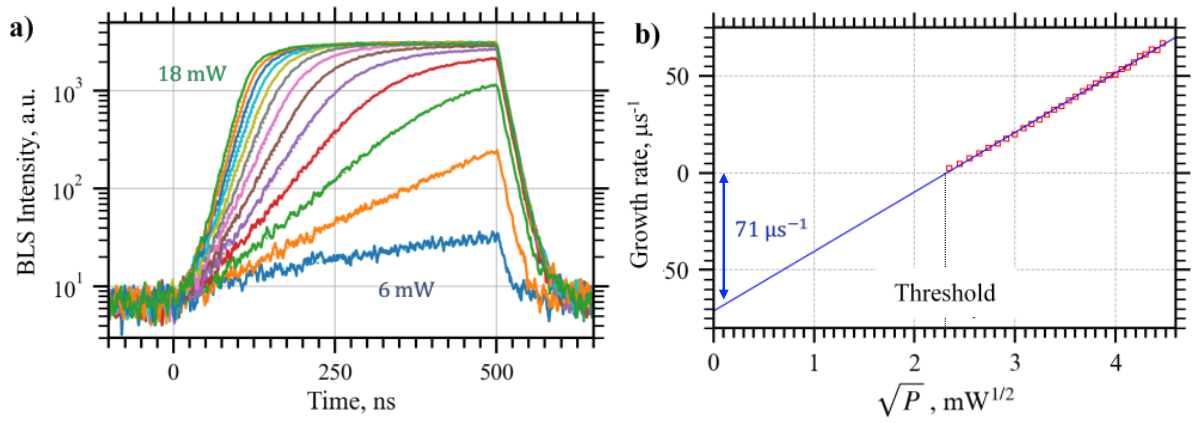

Figure 4: a) Temporal dependencies of the intensity of the spin-wave mode at the frequency 2.824 GHz for powers of the parametric pumping P increasing from 6 to 18 mW in 1 mW step. b) Rate of the exponential growth of the mode intensity as a function of $P^{0.5}$, which is proportional to the amplitude of the dynamic magnetic field of the pumping signal.

entire duration of the pumping pulse (500 ns). Under these conditions, the intensity of the excited mode can be easily controlled by varying the pulse width. Additionally, one obtains the possibility to switch between the linear and the nonlinear magnetization oscillation regime and control in this way the nonlinear coupling of the modes. At P>10 mW, the temporal traces of the intensity exhibit a clear saturation suggesting the onset of the nonlinear limitation, while the growth rate becomes large, indicating that the nonlinear regime can be achieved within a short time interval. In fact, the fastest achievable settling time of the mode intensity provides information about the achievable operation speeds of the networks driven by the parametric pumping. Measurements at the maximum used P=100 mW show that this settling time can be as small as 50 ns. We note that, at a given power of the pumping signal, the growth rate increases with the decrease in the natural magnetic damping. Therefore, by reducing the latter, one can achieve even larger operating speeds.

The time-resolved measurements of the growth rates additionally provide important information about the intrinsic properties of the investigated structures. In Fig. 4b, we plot the dependence of the measured growth rate as a function of $P^{0.5}$, which is proportional to the amplitude of the dynamic magnetic field of the pumping signal h. As seen from the data, in agreement with the general theory of the parametric excitation, the growth rate exhibits a linear dependence on $P^{0.5}$. By extrapolating this dependence, to P=0 and finding the intercept with the vertical axis, we determine the intrinsic relaxation rate of the spin-wave mode 71 μs^{-1}, which characterizes the natural damping of the magnetization oscillations. This value corresponds to the Gilbert damping constant for the studied YIG disk $\alpha_{disk} = 2 \times 10^{-3}$. This value is significantly larger than $\alpha = 8 \times 10^{-5}$ obtained for the YIG film before structuring. This result indicates that the structuring causes a significant increase of the damping, which can be avoided by optimising the fabrication process. Correspondingly, one can expect that such optimization will result in a significant improvement of the characteristics, such as the required microwave power and the reaction time of parametrically driven networks.

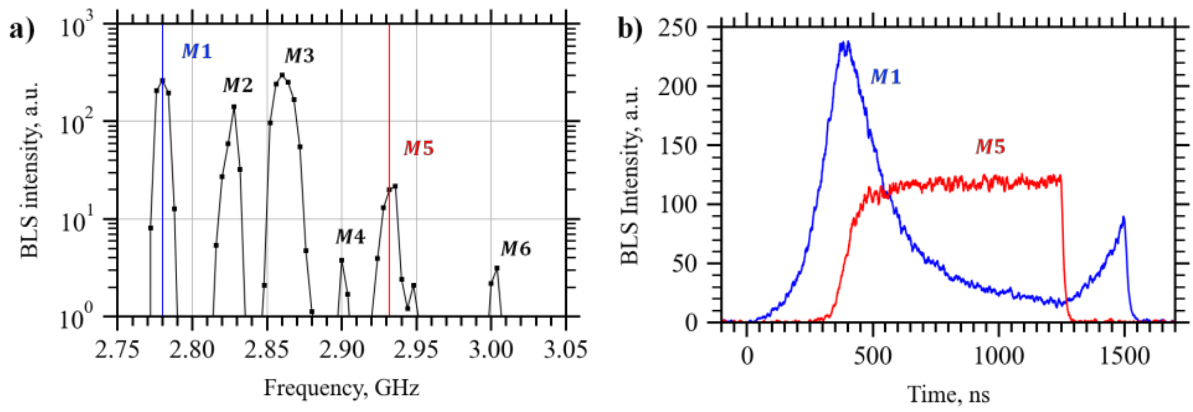

Figure 5: a) Spectrum of parametrically excited modes. b) Temporal dependencies of the intensity of the modes M1 and M5.

3 NONLINEAR INTERACTIONS OF PARAMETRICALLY EXCITED MODES

3.1 Indirect mode interaction

To prove whether the parametrically excited modes can efficiently interact with each other, we performed measurements, where two chosen modes were excited simultaneously and the mutual influence was studied. First, we address results obtained for the case, when the excited modes were well separated in the frequency space, which is expected to result in a relatively weak interaction. The typical behaviours observed in this case are characterized in Fig. 5. We parametrically excited the mode *M1* (see Fig. 5a) and then applied the second pumping signal to excite the mode *M5*. As seen from Fig. 5b, at the first stage, the intensity of the mode *M1* growths exponentially. As the second signal is applied after 250 ns, the intensity of the mode *M5* starts to grow, while the intensity of the mode *M1* quickly decreases. Finally, after the pumping of the mode *M5* is stopped after 1000 ns, the intensity of the mode *M5* drops, while the intensity of the mode *M1* starts to restore. These behaviours suggest that the excitation of the mode *M5* causes the suppression of the mode *M1*. This suppression generally becomes stronger with the increase of the intensity of the mode *M5*, which is controlled by the power of the second pumping signal. Similar effects were observed for other mode pairs.

We associate the observed effects with the influence of the second mode on the coupling of the first mode with its parametric pump. When a mode is parametrically excited, particular phase relation between the phase of the pump and that of the mode are established providing the optimum energy flow. As the second mode is excited, the eigenmode spectrum modifies due to the nonlinear renormalization. This results in a disruption of the optimum conditions for the coupling of the already excited first mode with its pump leading to the decrease of its intensity. This mechanism does not involve direct energy exchange between modes, but rather represents an indirect influence of the modes on each other due to modulation of their coupling with the pump. One of the advantages of this indirect mechanism is that it does not require the interacting modes to be close to each other in the frequency space. It only depends on the intensities of the interacting modes, which can be easily programmed by appropriately adjusting the intensities of the pumping signals.

3.2 Nonlinear phase locking of the modes

Our experiments showed that, in addition to the indirect interaction, the parametrically excited modes can interact directly, provided that their frequencies are sufficiently close to each other. These effects are illustrated in Fig. 6 for the case of the simultaneous excitation of the modes *M2* and *M3* (see Fig. 5). In these experiments, we first applied the pumping signal for the mode *M3* and then that for the mode *M2.* Additionally, we varied the frequency of the mode *M2* within the range 2.816-2.828 GHz, where the parametric excitation of this mode is observed (Fig. 5a). Figure 6a shows the temporal dependencies of the sum of the intensities of the modes *M2* and *M3* recorded for different frequencies of the mode *M2*. Here, one observes the reduction of the total intensity within the temporal interval 250-750 ns, where both modes are pumped simultaneously. This is due to the effects discussed in the previous section. Additionally, for the frequencies f_{M2} = 2.820 and 2.824 GHz, one observes an appearance of periodic oscillations with the frequency equal to the difference of the frequencies of the modes *M2* and *M3*, Δf (see the Fourier spectra in Fig. 6b). We emphasize that the phases of these two modes are not mutually locked by the excitation mechanism and change arbitrarily from one pumping pulse to the other. Therefore, in the case of non-interacting modes, one does not expect to observe a beating of the intensity at the difference frequency in stroboscopic measurements. Indeed, for the frequencies f_{M2} = 2.828 GHz and 2.816 GHz the oscillations become indistinguishable. The observation of the oscillations within a certain range of the frequencies and intensities of the modes clearly indicates that the parametrically excited modes become mutually coupled resulting in the locking of their phases. Although we do not yet have a rigorous theoretical model that provides an understanding of the physical mechanisms responsible for this coupling, we can definitely conclude that closely spaced modes can exhibit direct nonlinear interaction.

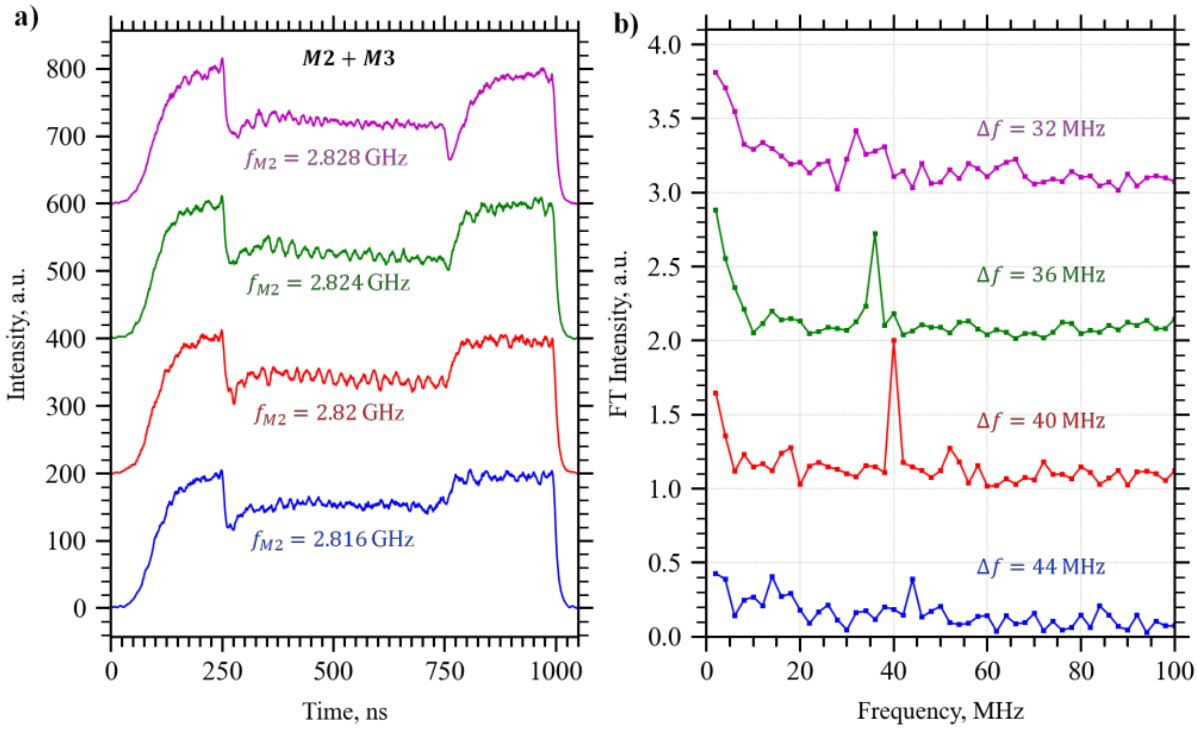

Figure 6: a) Temporal dependencies of the sum of the intensities of the modes M2 and M3 recorded at different frequencies of the pump for the mode M2. b) Fourier spectra of the temporal intensity traces in the time interval 250-750 ns.

Although, these were encouraging results to build the k-space the neural network, the non-linear interactions between two parametrically pumped modes seem to be dominated by the perturbation of their relation with the pump. Indeed, in simulations and in the experiments with the 2nd generation of sample with improved damping (received in December 2022 (M23)), direct scattering from parametrically excited modes is easily observed. Moreover, we point out that in the steady-state regime of parametric pumping, the energy of the pumped mode is necessarily re-distributed over other modes, thus synapses must be created. Although these hidden modes can contribute meaningfully to the computation as internal neurons, it is difficult to directly assess the corresponding synaptic weights and to study their control.

Consequently, in the follow-up research, we have investigated the magnetic system driven by a combination of strong direct and parametric excitation. The direct excitation allows us to put the system in a non-linear regime where direct interactions between modes are observed or promoted. We can then use parametric pumping to control the synaptic weight or even to create new synapses.

4 PROGRAMMING WITH PARAMETRIC PUMPING STIMULATION

In the first part, we describe the experimental set up and the observation of the efficient scattering of magnons from one mode to another or to multiple modes above a certain threshold, through a process, which can be treated as the modulation instability or four-magnon scattering.

In the second part, we measure the effects of using a secondary parametric excitation to control the scattering between the modes. We separate two cases:

i. a secondary parametric excitation below or near the parametric threshold
ii. a secondary parametric excitation above the parametric threshold

We demonstrate that the secondary source can stimulate the spontaneous scattering initiated by the primary source and thus control the synaptic weights of pre-existing synapses connecting different neurons. We also demonstrate that a secondary source can also mediate the creation of additional synapses between modes.

4.1 Observation of spontaneous scattering

In the measurements described below, we used the same samples prepared within WP1 of the k-NET project (described in detail in the technical report D1.1). In this section, two microwave-frequency sources are connected to the antenna via a power combiner (see Fig. 7) and are applied simultaneously in 1-µs pulses (unless specified otherwise). The static magnetic field H_0 is applied at a 45° angle to allow the efficient excitation of spin waves both with direct-excitation (Source 1) and parametric-pumping (Source 2) mechanisms. H_0 is set at 15 mT.

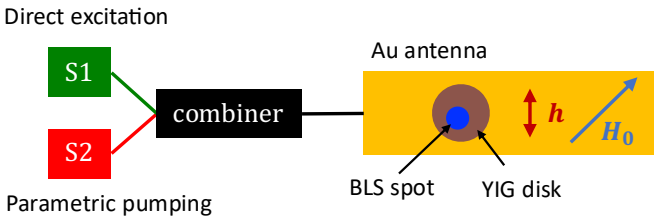

Figure 7: Schematics of the experiment. Two rf-sources provide an rf-current to the wide antenna patterned on top of the 1-µm disk. The static magnetic field H_0 is oriented at 45° with respect to the microwave field h of the antenna, allowing both transverse and parametric excitation of the magnetization dynamics. The magnetization oscillations are measured using µ-BLS.

First, only the direct excitation is applied to put the magnetic system into a non-linear state. Figure 8 shows the spin-wave amplitude (square root of the BLS intensity) as a function of the frequency of the primary excitation source S1 (f_1 from 1.05 to 1.75 GHz with a 5 MHz spacing on the y-axis) for 4 different powers: 5, 12, 14, 20 dBm.

At low power ($P_1 = 5$ dBm), the system is in the linear regime and the spin waves are excited at resonance, i.e. only at the frequency of excitation. The fundamental mode is excited around 1.59 GHz at an applied field $H_0 = 15$ mT. From simulation and our previous experiments with parametric pumping, we know that bulk modes of the 1-µm disk are located within less than 100 MHz or above the fundamental mode. Thus, we identify the bright spots around 1.3 - 1.4 GHz as corresponding to different edge modes.

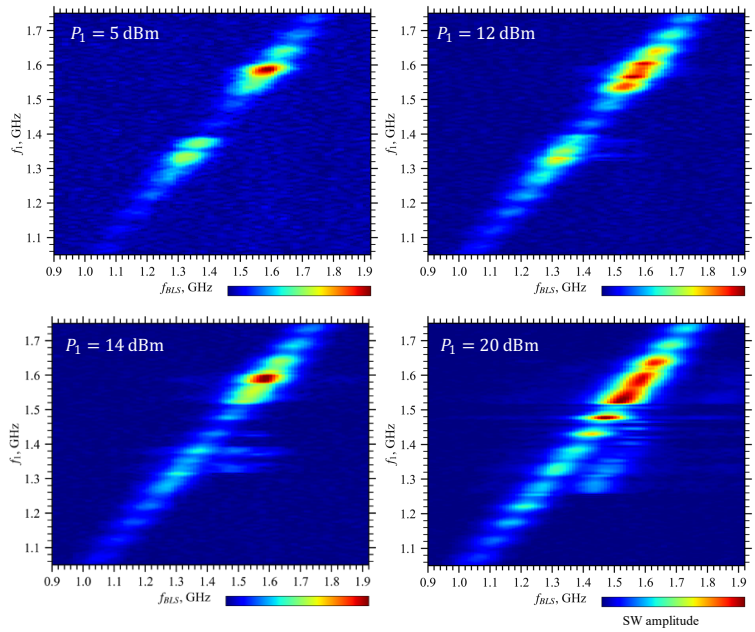

Figure 8: Color maps of the SW amplitude obtained from the BLS spectra as a function of the applied frequency f_1 (y-axis) at different applied powers $P_1 = 5, 12, 14, 20\ dBm$. At low power, only a resonance at f_1 is detected (white dotted line). At increased powers, the magnon scatter from the resonant mode to other modes.

When the power is increased to 12 and 14 dBm, off-diagonal spots appear on the maps. This indicates that magnons can scatter from the excited mode to other discrete modes. As the power is increased to 20dBm, the resonance of the fundamental mode forms a plateau as it shifts down in frequency. We start to reach the deep non-linear regime in which the concept of orthogonal mode computed from the linearized LLG equation starts to fall apart.

There are two alternative ways to interpret the observed scattering, either in the time or in the frequency domain. In the time domain, the large intensity of a mode can locally change the internal magnetic field, which in turn changes the profile of the mode and results in additional changes of the internal magnetic field. This self-action process can be unstable and can lead to a temporal modulation of the spin-wave envelope that can be periodic or even chaotic. This process is usually referred to as dynamic instabilities, modulation instabilities or self-modulation. In particular, it was studied within the consortium at the CEA using MRFM on an out-of-plane magnetized Bi-YIG disks with perpendicular uniaxial anisotropy. It was demonstrated that the negative non-linear frequency shift leads to an early saturation of the precession angle and thus a plateauing of the resonance due to dynamic instabilities. On the contrary, in the in-plane magnetized disks with positive non-linear frequency shift, the self-interaction of the mode with the internal field is stable and large precession angles can be reached. Similarly, when we performed our experiments for the out-of-plane field configuration (positive non-linear frequency shift), no scattering was observed. Instead, we observed a well-defined foldover-like resonances. Although the μ-BLS has the time resolution to study such phenomena, these instabilities occur with a random phase. Thus, even single sweep of the BLS only gives the magnetization oscillations averaged over many repetitions of the dynamic instability.

Nevertheless, the μ-BLS provides direct access to the frequency-domain picture of this phenomenon. When the fundamental mode f_1 is excited above a certain threshold amplitude, its energy is redistributed via four magnon scattering within the magnon bands. As frequency $f_1/2$ falls within the magnon gap (no available modes), three-magnon scattering processes are absent in the disk at the applied frequencies. Thus, the leading non-linear mechanism is four-magnon scattering. In this process, the annihilation of two magnons at f_1, leads the creation of a first pair of magnons (f_+, f_-) under conservation of energy. These magnons can themselves scatter with a magnon at f_1, creating a cascade of scattering at different orders such that:

$$f_{\pm}^{n} = f_1 \pm n * \Delta f_0$$

We note that in the experiment, not all modes $f_{\pm}^{n}$ are resolved. This could be due to the strong decrease of the BLS sensitivity for large k-vectors. Furthermore, it is not guaranteed that the scattering is resonant. Indeed, in the case of a microscopic disk, there might not be modes available at scattering frequencies and non-resonant scattering might dominate.

4.2 Parametric threshold

Before applying a secondary parametric excitation, we determine the parametric threshold power of the modes in this configuration. The BLS intensity at half the excitation frequency is showed in Figure 9. At $P_2 = 17$ dBm (blue curve), only edge modes below 1.25 GHz are excited. At $P_2 = 21$ dBm (red curve), both the edge modes and the fundamental mode are just slightly above threshold. At $P_2 = 25$ dBm, all the edge modes and the bulk modes around the fundamental mode are well above the threshold. We underline that no spontaneous scattering from the parametrically excited modes is detected at these microwave powers.

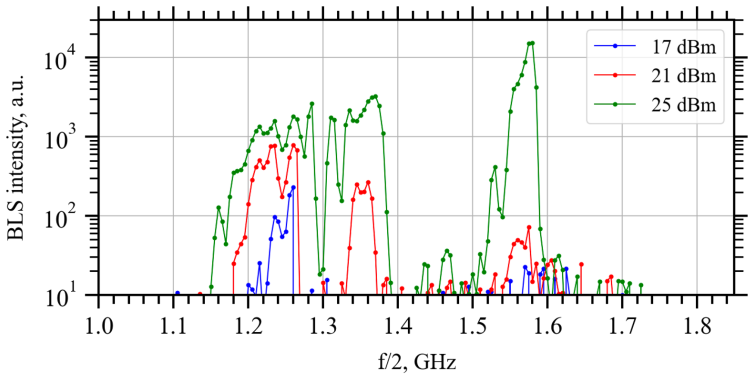

Figure 9: BLS intensity at f/2 from parametric pumping at different applied powers $P = 17{,}21 \text{ and } 25\ dBm$.

4.3 Scattering stimulated by parametric pumping

The first rf-source (S1) is now set at a power $P = 14$ dBm, corresponding to a power where we observe scattering from edge modes into the fundamental mode and into two modes at the same time around 1.37 GHz. The second rf-source (S2) is turned on and emulates either the parametric excitation of an input neuron, or another program neuron whose role is to control the synaptic weights. Both sources are applied simultaneously in 1-µs pulses.

a) Parametric pumping below or at threshold

The frequencies of both sources are swept and the resulting BLS spectra are agglomerated in color maps, as shown in Figure 10.

First only S1 is turned on (Fig. 10 a) and its frequency is swept between 1.05 and 1.75 GHz. At this power, the spontaneous scattering is concentrated in a region between 1.32 and 1.38 GHz. This measurement is

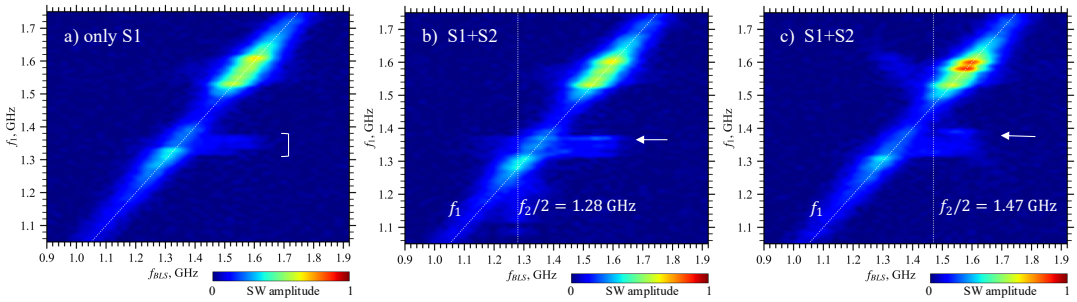

Figure 10: Color maps containing the BLS spectra as a function of the excitation frequency f_1 for a single source with power $P_1 = 14\ dBm$ (a) and for two sources with $f_2/2 = 1.28\ GHz$ (b) and $f_2/2 = 1.47\ GHz$ $P_2 = 21\ dBm$ (c). For a single source, magnons scatter in a narrow region (white accolade). The second source generates a second resonance at f_2 (vertical dotted line) and noticeably influences the scattering (white arrows).

then repeated for each frequency $f_2/2$ between 1.05 and 1.75 GHz, thus producing 61 color maps. Two examples of such color maps are shown in Figs. 10 (b,c), for frequencies $f_2/2 = 1.28\ \mathrm{GHz}$ and $f_2/2 = 1.47\ \mathrm{GHz}$, respectively.

We use these maps to identify the region where the presence of S2 can increase the intensity in the scattered modes and extend the frequency range of efficient scattering (see white arrows in Figs. 10 b,c).

The application of a the parametric pumping at f_2 can typically stimulate the spontaneous 4-magnon scattering process as shown in Figures 11 where $f_1 = 1.37\ \mathrm{GHz}$ and $f_2/2 = 1.28\ \mathrm{GHz}$ (a), $f_2/2 = 1.46\ \mathrm{GHz}$ (b,c) and $f_2/2 = 1.57\ \mathrm{GHz}$ (d). Strikingly, at 17 dBm (a,b) even though the mode at $f_2/2$ is below the parametric threshold (see flat red curve where S2 is applied alone), a strong stimulation of the scattering up to the 3rd order is observed (black curve, where S1 and S2 are applied together).

When the power of the stimulation is increased to 21 dBm for $f_2/2 = 1.46\ \mathrm{GHz}$, the population in the fundamental mode (2nd order scattering) doubles again (see Fig. 11 c). Although this power still corresponds to a sub-threshold power at this frequency, it is sufficient to significantly change the non-linear coupling between the modes.

It is also possible to strongly excite the fundamental mode at low parametric power thanks to the scattering (Fig. 11 d). The observed strong increase in the magnon population can be associated with either a lowering of the parametric threshold due to the four-magnon scattering or with the stimulation of the scattering by the flow of magnons from the parametric pumping. Hence, similarly to the direct excitation, a secondary parametric pumping can be used to control the weights of pre-established synapses. The quantitative evaluation of the synaptic weights is possible by scanning the power P_2 and detecting the time-resolved evolution of the respective populations.

Moreover, by analyzing the color maps generated by the scanning of both frequencies f_1 and f_2, we find that sub-threshold parametric pumping can also trigger the scattering between modes that otherwise would not scatter into any detectable mode. The results are presented in Fig. 12 for frequencies $f_2/2 = 1.43\ \mathrm{GHz}$ (a,b,d,e) and $f_2/2 = 1.46\ \mathrm{GHz}$ (c,f).

On all these color maps, the resonance at frequency f_1 is clearly visible and forms a line along the $f_{BLS} = f_1$ diagonal. No resonance is visible at $f_2/2$ as the power applied is below the parametric threshold. However, we observe a sizable BLS intensity along the anti-diagonal, corresponding to the symmetric of the f_1

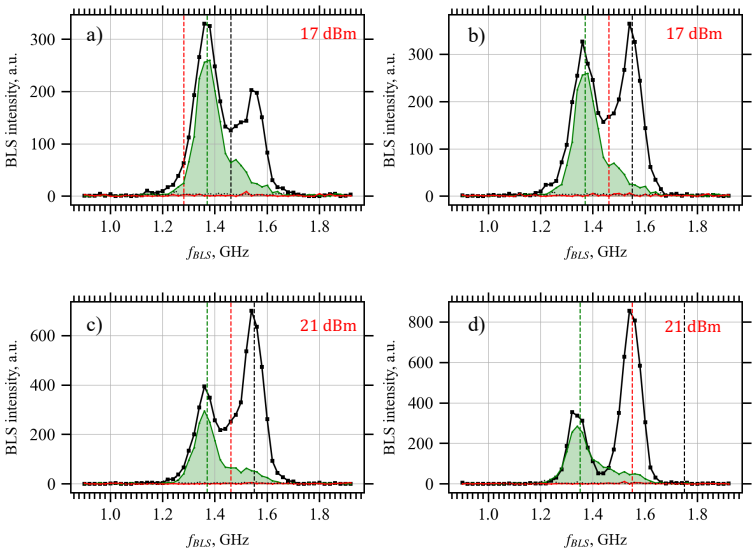

Figure 11: BLS spectra for different pairs (f_1, f_2) applied simultaneously (black curves). (a,b,c,d) $f_1 = 1.37\ GHz$ (green line) and $f_2/2 = 1.28\ GHz$ (a), $f_2/2 = 1.46\ GHz$ (b,c), $f_2/2 = 1.57\ GHz$ (d). S2 stimulates the scattering despite the low parametric power (red curves represent the measured spectra when S2 is applied alone).

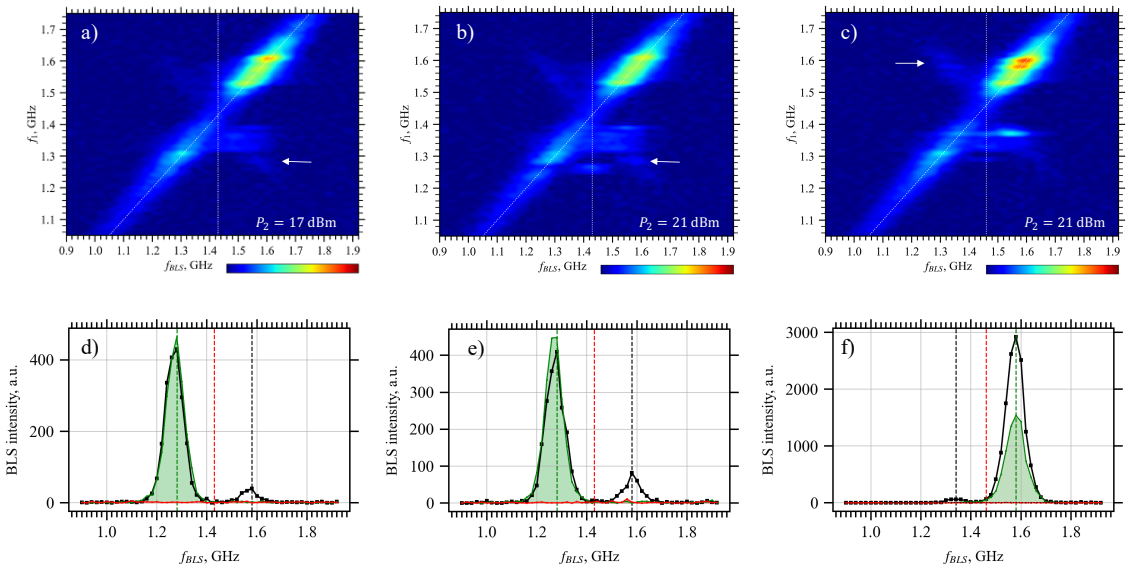

Figure 12: (a,b,c) BLS spectra as a function of the excitation frequency f_1, for $f_2/2 = 1.43\ GHz$ and $P_2 = 17\ dBm$ (a), $P_2 = 21\ dBm$ (b) and for $f_2/2 = 1.46\ GHz$, $P_2 = 21\ dBm$. Magnons scatter along the anti-diagonal $f_{BLS} = f_2/2 + (f_2/2 - f_1)$. The BLS spectra shown in (d,e,f) correspond to the conditions indicated by the white arrows.

resonance by the $f_{BLS} = f_2$ vertical line, in two regions: that of the fundamental mode (1.45-1.6 GHz) and that of the edge mode that is always below the spontaneous scattering region (1.2-1.3 GHz for $P_1 = 14$ dBm). Thus, the sub-threshold parallel pumping at f_2 allows magnons to scatter into:

$$f_{scatter} = f_2/2 + (f_2/2 - f_1)$$

The edge mode scatters into the fundamental mode and the fundamental mode can now scatter into the edge modes above EM0 around (1.3-1.45 GHz).

The graphs in Fig. 12 (d,e,f) show the BLS spectra representing the horizontal sections of the color maps under conditions indicated by the white arrows. These data show that increasing P_2 from 17 dBm (d) to 21 dBm (e) leads to a nearly doubling of the population in the scattered mode. The intensity of the scattered mode is also significant for the case $f_2/2 < f_1$ (Fig. 12 (f)) (note different scale of the vertical axis).

We underline that this effect is never observed in the case of direct secondary excitation at any P_2 power. The use of parametric pumping can thus mediate the non-linear coupling between two modes via a "dark mode" that has no detectable population and does not contribute to the BLS read-out. Furthermore, it affects modes of interest such as the main bulk modes that one can clearly distinguish in Fig. 12 (c), or modes that otherwise do not scatter at all or at least do not scatter into detectable modes.

We note that, in the used range of P_1 power, all bulk modes exhibit a negative non-linear frequency shift, while the edge mode that shows spontaneous scattering (1.3-1.45 GHz) exhibits a positive shift. It is known that the non-linear shift strongly affects how the mode precession locally modulates the internal field. Magnon modes that shift down in frequency, tend to self-localize, which can favor self-modulation starting from a certain threshold (behaviors observed for the fundamental mode in the deep non-linear regime in the previous part). On the opposite, modes that shift up in frequency tend to extend their spatial profile. In the case of bulk modes, this favors their stability at high powers. However, in the case of edge modes, this might favor their scattering into bulk modes. In other words, by using a strong direct excitation or a low-power parametric pumping, we now can control the non-linear coupling of modes that possess negative and positive non-linear frequency shift.

b) Parametric pumping above threshold

The second source power is now set at $P_2 = 25\ \mathrm{dBm}$ that is above the threshold for all edge modes (below 1.5 GHz) and bulk modes around the fundamental mode.

In this regime, sweeping both frequencies yields very rich nonlinear scattering behaviors, as demonstrated by color maps shown in Figures 13 (a,b). Here, we also observe mechanisms discussed in the previous section for sub-threshold powers: the second source can stimulate the spontaneous scattering in the 1.25-1.4 GHz frequency region (white accolade). As before, the increase of the power P_2 results in the increase of the scattering strength and in the increase of the frequency range where the scattering is observed. Moreover, we clearly see the same anti-diagonal intensity spots corresponding to a "dark-mode" process (indicated by red arrows). However, the significant difference is that now for most (f_1, f_2) combinations, the intermediate mode exhibits a noticeable intensity ("bright mode"). We also notice a significant extension of the frequency range, where the phenomenon is observed (up to 1.6-1.7 GHz) (Fig. 13 b).

Additionally, in the entire used range of (f_1, f_2), we detect a strong change in magnon population, whose characteristics do not correspond to any of the mechanisms discussed in the previous sections (indicated by a white arrow in Fig. 13 b). The BLS spectrum for these conditions is shown in Figure 13 (c). The system is excited at $f_1 = 1.24\ \mathrm{GHz}$ and $f_2/2 = 1.46\ \mathrm{GHz}$. Under these conditions, the parametric pumping is expected to excite the mode at $f_2/2$ (see the red spectrum corresponding to the case when S2 is used alone). However, when both frequencies f_1 and f_2 are applied together (black curve), we observe no resonance peak at $f_2/2$, but rather an increased population in two modes (black dashed vertical lines) on each side of $f_2/2$ (red vertical dashed line). These modes can correspond to the 1st or 2nd-order scattering from f_1. The stimulation could come from a non-degenerate 3-magnon splitting process of the excitation at $f_2/2$. In other words, in the presence of f_1, the non-degenerate parametric process could have a lower threshold than the degenerate one.

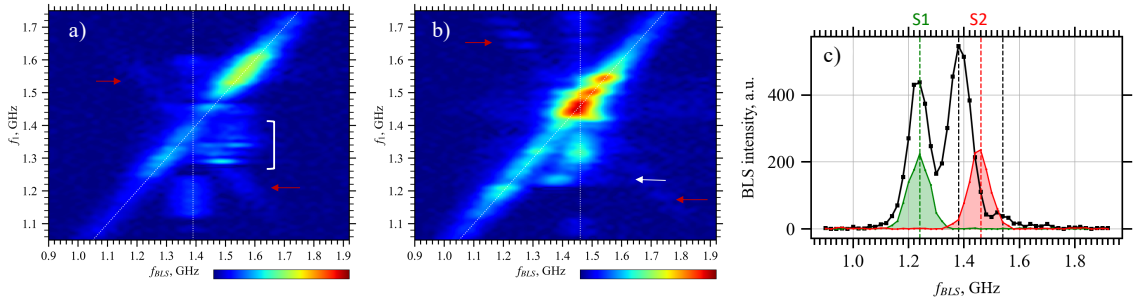

Figure 13: BLS intensity as a function of frequency f_1 for $f_2/2 = 1.39\ GHz$ (a) and $f_2/2 = 1.46\ GHz$ (b,c) and $P_2 = 25\ dBm$.

5 CONCLUSION AND OUTLOOK

To conclude, we have successfully performed studies planned for the Task 2.1 of WP2, which created a solid basis for the further progress of the project implementation. In particular, in agreement with the initial plan, we have demonstrated efficient controllable parametric programming of large number of spin-wave modes in microscopic ferromagnetic structures. We have observed how parametrically driven modes can control and create synapses in the k-space neural network when the system is set in a non-linear state using a direct excitation.

As the next step, we will analyse the possibility to implement advanced programming by additionally utilizing complexe waveforms. We will also develop theoretical models, which will allow us to understand deeply the observed nonlinear interactions and find optimum ways for their utilization in k-space networks. Additionally, the obtained results indicate the importance of optimization of fabrication techniques to reduce the adverse effects of the patterning on the damping of magnetization dynamics, a task that has been carried out and described in **D1.2**